Chapter 2

Band Structure, Morphology, Functionality, and Size-Dependent Properties of Metal Nanoparticles

Joseph Adeyemi Adekoya,
Kehinde Olurotimi Ogunniran,
Tolutope Oluwasegun Siyanbola,
Enock Olugbenga Dare and Neerish Revaprasadu

Additional information is available at the end of the chapter

http://dx.doi.org/10.5772/intechopen.72761

Abstract

Metallic nanoparticles are gradually emerging as important materials because of their novel shape and size-dependent chemical and physical properties that differ drastically from their bulk counterparts. The main challenges in the field of nano-chemistry are the rational control and manipulation of synthesis to derive materials with one of their dimensions in nanometer regime, and upscale production of nanomaterials for device fabrication. This chapter reviews the fundamentals of the quantum properties of metals and quantum mechanical size effects with special focus on clusters of Pd, Pt, Au and Ag. Effects of reduction in size of metal nanoparticles to nanoscale on their various properties (structural, thermal, mechanical, chemical, electronic, magnetic and optical) are reviewed. The chapter concludes with a review of select medical applications of metal nanoparticles.

Keywords: metal nanoparticles, quantum theory, density functional theory, finite size effects, vacancies and dislocations, medical applications

1. Introduction

The discovery and development of novel materials has led to rapid industrial and technological use of these materials [1]. It has produced synergistic effect between scientific discovery and astronomical technology growth. More recently, the ability to 'synthesise-up' nanoscale architectures and components has given rise to the field of 'nanochemistry' the preparation and manipulation of molecular structures on a length-scale of 0.1–100 nm [2]. This phenomenal breakthrough has been achieved by exploiting the properties of materials at the nanoscale

dimension. As a result, nanoscience is producing in-depth knowledge of the properties of matter as it transforms from bulk to nano-phase, in which state, most of the properties differ from the conventional atomic or bulk phase. Meanwhile, it is imperative to understand the properties of matter as atom, molecule, or crystal in the bulk phase in order to gain an appreciation of the quantum properties of nanomaterials.

The diversity of the physical and chemical properties of inorganic nanoparticles can be attributed to phase transformation which has significantly affected the arrangement of the constituent atoms in a way that leads to quantization of energy levels. An understanding of this can be obtained from the chemistry of atomic structure which is discussed in details in many textbooks on Quantum Mechanics and Quantum Chemistry [3–6].

The ability to synthesise and process nanomaterials or nanostructures is an essential aspect of nanotechnology. The study of new physical properties and applications of nanomaterials or nanostructures are possible only when nanostructured materials are made available with the desired size, morphology and chemical composition. However, nanoparticles of noble metals have a history of fundamental synthetic strategies known for some decades. A number of synthetic routes have been developed for metal nanoparticles which emanate from the knowledge of small particulate as earlier mentioned. The main objective of which is to obtain monodisperse metal particles with high degree size, structure and composition functionalities, diameters ranging from 1 to 100 nm, consistent crystal or amorphous structure, large surface area to volume ration and a high degree of mono-dispersity. Moreover, one of the challenges encountered in this process is the need to control the size of nanoparticles. Among the synthetic methods developed, gas-phase technique would have been one of the best with respect to size and mono-dispersity but for the high reaction temperature which often leads to uncontrolled particle size during anisotropic nucleation and nanoparticle growth. Rigorous control over reduction, nucleation-condensation and growth, as well as effective purification and isolation methods ensure monodispersed nanoparticles with tunable morphological properties. The homogeneity of metal nanoparticles and their ability to resist agglomeration, sintering, and flocculation can be enhanced by re-dispersing the nanoparticles in solution. However, polar solvents and surfactants have been used to stabilize semiconductors and metallic nanoparticles respectively in most syntheses aimed at producing monodispersed nanoparticles. In the preparation of nanomaterials, organic compounds are known to play similar role as surfactants in the processing of mesoporous materials. In this chapter, some fundamental principles are first considered in order to rationalise the concept of quantum size effect in the evolution of properties of materials at the nanoscale level.

2. Crystalline solids and their periodicity

In the above, it has been stated that properties of materials change as the materials transform from bulk to nano-phase. Let us consider a crystalline solid having a three-dimensional system, in which the electronic properties of bulk crystalline solids can be rationalized based on existing principle of the eigen wave-functions, φ. For a perfectly ordered three-dimensional

crystal, the periodic repetition of atoms (molecules) along the one dimension is replaced by three-dimensional repeating unit cell. The unit cell is made up of atoms arranged in the characteristic crystal structure, such that repeating unit cells in all the space are enough to form the entire crystal structure. Consequently, the crystal has translational symmetry because the structure of the crystal can be generated by translation of the unit cell in all three dimensions. Translational symmetry in a periodic structure is also referred to as discrete symmetry because only certain translations that correspond to integer multiples of the lattice translation vectors derived from the unit cell lead to symmetry equivalent points. Invariably, the weak discrete translation symmetry in crystals leads to a weaker quasi conservation law for quasi or crystal momentum. This discrete translation symmetry can be used to give an account of the electronic properties of crystals which is described by Bloch's theorem [7].

A brief rationalization of the Bloch's theorem is hereby considered. In a crystalline solid, the three-dimensional periodicity of the atomic arrangement gives rise to a corresponding periodicity in the internal electric potential due to the ionic cores. When this periodic potential is incorporated into the Schrodinger equation, the outcomes are certain allowed wave functions that are modulated by the lattice periodicity. Bloch's theorem therefore states that these wave functions appear in form of a plane wave. Such wave functions are known as Bloch functions and represent travelling waves passing through the crystal but with a form modified periodically by the crystal potential due to each atomic site.

The two important inferences drawn from Bloch theorem are (i) the volume of k-space occupied by each wave-vector state in one-dimension (1D) is $2\pi/L$; for a three- dimension (3D) crystal, a k-space volume is $8\pi^3/L^3$ and (ii) the number of wave-vector states contained within each energy band. The lattice periodicity also gives rise to diffraction effects which is a key characterization tool in solid state materials. It is well known that electrons possess wave-like properties, therefore, the free electrons in the crystal would experience diffraction effect which invariably affects the spectrum of apparent electron energies.

We imagine an electron travelling along a one-dimension chain of atoms of spacing a, where each atom would generate a reflection of the wave. These reflections can be reproduced if $m\lambda = 2a$, for a given m, λ is de Broglie wavelength for the electron. Given this condition, both the forth and backward traveling waves coexist and can be superimposed over each other creating standing waves. The standing waves give rise to electron density distributions of the order $|\varphi(x)|^2$ having either nodes or antinodes at the lattice sites x = a, 2a, 3a,…. These solutions may have the same wave-vector value but they definitely have different energies domains as a result of different interaction between the energy level of electron and the positively charged ions. As a result, a band gap appears in the electron dispersion curve corresponding to certain values of wave-vector [3].

3. Morphological properties of metals

As mentioned earlier, understanding the structure and mechanical properties of nanostructured materials is important for the manipulation and modification at the atomic level.

Increasing the number of atoms from a single one via a cluster to the bulk, one finds 'magic number' which corresponds to crystalline structures of high stability. These are reflected, for example by peaks representing different clusters of various sizes. In the case of rare gas clusters with an isotropic atom interaction potential, the stable configurations correspond to a dense packing of atoms, for instance, icosaeders around a central atom with increasing particle numbers ('magic numbers' of 13, 55, 147…). With increasing size, these five-fold symmetries show more and more defects. In the case of argon one observes at about 1000 atoms the crystalline structure of the bulk solid.

For more complex atoms such as metals, with anisotropic interaction potentials or open shells the morphologic rules become more complicated. For large clusters magic numbers exist, but for smaller clusters electronic effects dominate. In this range of smaller clusters the closed electronic shells (N = 8, 18, 20…) result in most stable clusters [8]. As it were, it would be interesting to observe simple morphologic rules since crystal structures are affected by small changes in the long range interaction potentials. For aggregates with dimensions of the order of several atom distances, a strong influence of these 'surface' effects is expected and stability of such an aggregate cannot be easily predicted. Moreover, it is possible to calculate or measure the resulting structures for a given number of atoms or better still deduce the structure of a nanoscaled aggregate of given dimensions and determine whether such a structure is stable or not. In this context the most important structures are these connecting elements between specific aggregates, for example, simple wire. An important question is how thin could this wire be?

The mechanical properties of a wire of individual gold atoms have recently been investigated by a combination of scanning tunnelling microscopy (STM) and an atomic force (AFM) sensor [9]. The gold wire was connected between the force microscope tip and the golden tip of an STM. The force necessary to stretch the wire was then determined with the help of a second STM which detected the extension of the AFM tip. The surprising result was that the bond strength between the atoms in the nanowire was twice that of the bond strength in the bulk. Apparently, the effective stiffness of a nanostructure depends on the exact configuration of the atoms at the base.

4. Electronic structure and optical properties of metals

Quantum mechanical size effects occur if the size of a crystal or particle approaches the characteristic length scale which determines the coherence of its wavefunction. At or below this size the electronic, optical and magnetic properties become size-and shape-dependent. In particular, the optical behaviour is very sensitive to quantum effects otherwise called 'quantum confinement'. The significance of the effects depends on the temperature and the distance between neighbouring energy levels or bands which has to be large compared to thermal energy, k_BT, in order to avoid a smear-out of the effect by thermal fluctuations.

The absorption of a photon results in an electron–hole pair in the material, precisely a quantized state called exciton. In semiconductors, due to the small effective masses of electrons, m_e, and hole, m_h, (effective meaning the masses in the presence of the lattice) and the large

http://dx.doi.org/10.5772/intechopen.72761

dielectric constant ϵ, the exciton is large on the atom scale, with Bohr radii a_0 between 5 and 50 nm. The Bohr radius of an exciton is given by

$$a_0 = \frac{h^2 \in}{e^2}\left[\frac{1}{m_e} + \frac{1}{m_h}\right] \quad (1)$$

If the semiconducting aggregate reaches one (quantum gas), two (quantum wire) or three dimensions (quantum dot engineered by self-assembly on a substrate) [10] a size that is comparable with a_0 or the de Broglie wavelength $\lambda_{dB,}$ substantial changes in the optical properties are observed. In metals however, such effects are observed only for very small aggregate of a few nano-meters on account of the missing band gap and the corresponding small distances between relevant energy levels [11, 12].

4.1. Electronic conduction as it relates to different geometry in crystal systems

In three-dimensional crystal, the location of energy band gaps in the electron dispersion is still determined from electron diffraction by the lattice planes, but the Brillouin zones (which is the region of k-space which lies between any two diffraction conditions, where k = −π/a and +π/a in one dimension) don't exist as simple variables of k, as in 1D but, they exist as more diverse surfaces in 3D k-space, which geometry depends on the unit cell and atomic structure. The energy-wave-vector relationship for this crystal which extends over multiple Brillouin zones when mapped completely into the first Brillouin zones, results into a large number of energy bands and consequently the density of energy states (DOS) is strongly modified (**Figure 1**).

An example of the multiple energy bands and corresponding density of states in a real crystal is shown for Ag_2ZnGeO_4 crystal in **Figure 2a**.

The series of allowed k values extend up to the edge of the Brillouin zone, at k = ±π/a since one of these endpoints may be mapped onto the other by a reciprocal lattice vector translation. The total number of allowed k values is precisely N, where N is a positive integer. Meanwhile, each k state may be taken up by both (+) spin or (−) spin electron, where the total number of states to be occupied is 2N per energy band. In three dimensional states, this result is translated to $2N_u$ states per band where N_u represents the number of unit cells in the crystal.

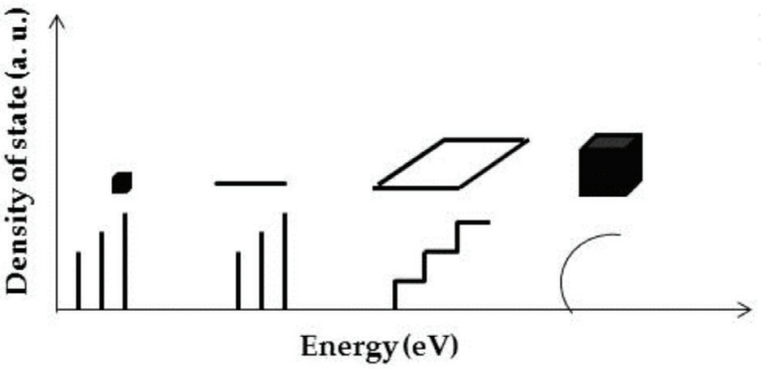

Figure 1. Electronic densities of state for nanostructures of various dimensions (reproduced with permission from Ref. [13]).

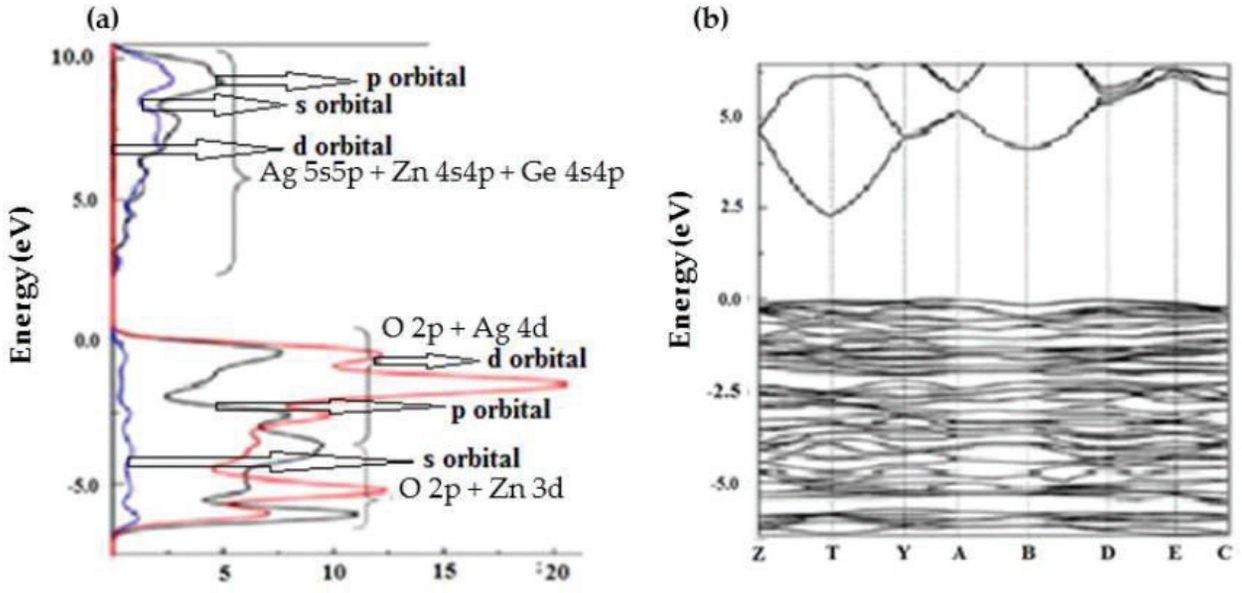

Figure 2. (a) Density of states for crystalline Ag_2ZnGeO_4 showing the symmetry along the Brillouin zone boundary (b) diagram of electron energy band gap structure (reproduced with permission from Ref. [14]).

Therefore, the sum of valence electrons in the crystal is zN_u, where z is given as the valence electron per unit cell, leading to two different electronic configurations in a crystalline solid.

For an even integer of z, one energy band will be fully filled, while the next band will be completely empty (**Figure 2b**). Apparently, the valence band is the highest densely filled band while the conduction band is the next unoccupied band. It is impossible for electrical conduction to occur in the valence band because there are no unoccupied states equivalent to the small increase in energy due to externally applied voltage. This phenomenon results in an insulator, but if the band gap is considerably small, a semiconductor is formed. Conversely, if z is an odd integer, the highest occupied energy band will be half filled and there will be many unoccupied states with comparable energy to the highest occupied states. This invariably results in vigorous electrical conduction typical of a metal material.

There is one further special case which gives rise to metallic behaviour, namely, when the valence band is completely full (z is even), but the valence and conduction bands overlap in energy, such that there are vacant states immediately adjacent to the top of the valence band, just as in the case of a half-filled band. Such a material is called a semi-metal or metalloid. Moreover, in amorphous solid DOS is primarily determined by the short-range order in the material, that is, the nearest neighbours. Another approach is to represent the amorphous solid by a very large unit cell with a large number of slightly different atomic environments [15, 16].

4.2. Properties of metal clusters

Over the past decades, researchers have been interested in studying nanoparticles and/or small clusters of noble metal materials in which the system sizes under investigation have been experimentally synthesized, which enables direct theory-experiment comparison. More often, the size-dependence of the properties of these materials such as their HOMO-LUMO gap (**Figure 3**), magnetic properties and optical properties are of immense interest.

http://dx.doi.org/10.5772/intechopen.72761

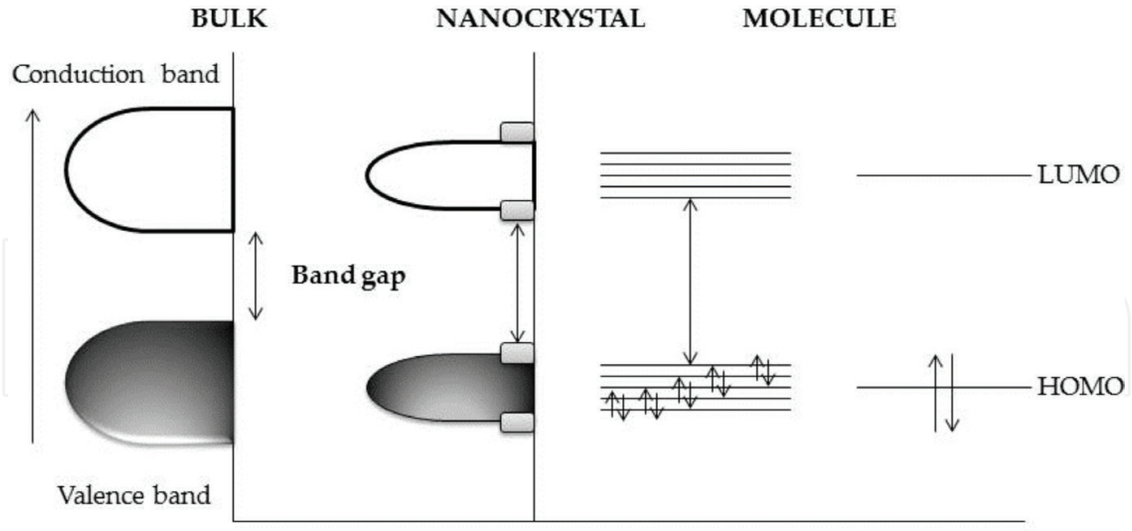

Figure 3. Band structures of bulk and nanoparticles.

Therefore, computational methods employ time-dependent density functional theory (TDDFT) using either the linear response (LR) formalism of Casida or a real-time (RT) approach to calculate the excited-state in solid crystals. The TDDFT calculations usually employ the adiabatic local density approximation (ALDA) which is sometimes referred to as the time-dependent local density approximation (TDLDA). Recent model potentials used in TDDFT calculations include the asymptotically correct exchange functional (LB94) [17]. Like all DFT calculations, the results depend on the type of system and the particular exchange-correlation functional employed. We shall briefly consider some model noble metal systems and the implications of DFT studies on their structure and DOS or band gap energy.

4.2.1. Pd clusters

Palladium is of immense interest due to its many uses in applications such as fuel cells and catalytic converters. The properties of palladium clusters and nanoparticles have been studied by many researchers, who investigated 13-atom Pd metal clusters [18]. They used the linear combination of atomic orbitals method for their calculations within the density functional formalism, at the same time, the von Barth-Hedin form was also used to include the exchange correlation effects in their calculations. In concluding, it was discovered that the icosahedral geometry is more stable for Pd_{13} than the face-centred cubic (fcc) octahedron, and it has a nonzero magnetic moment unlike the bulk, which is diamagnetic. In addition, the binding energy per atom of the 13-atom Pd cluster was calculated and compared to the bulk cohesive energy. Other researchers also reported the icosahedron structure as the most stable isomer for Pd_{13} [19] but, the final structure was found to be a distorted icosahedron with D5d symmetry with a zero spin only magnetic moment. Furthermore, the mutual dependence between electronic structure and geometric characteristics of small Pd clusters was equally measured using the self-consistent-field/configuration interaction (SCF/CI) level of theory.

By extension, the cuboctahedral and icosahedral symmetries of Pd_{13} were studied to explore its atomic and electronic structures by means of the linear combination of norm-conserving

pseudopotential atomic orbitals (LCPSAO) method with both PZ and PBE exchange correlation functionals. It was found that the cuboctahedral Pd^{13} is more stable with a small spin polarization, S = 3. The accuracy of the numerical calculation and the treatment of the core electrons were attributed to account for the difference observed in contrast with previous studies [20].

A low symmetry structure with relatively close packing has been identified as the lowest energy isomer using the DFT-PW91 level of theory for the Pd_{13} cluster. It was discovered that the structural orientation of Pd closely resembles that of noble metals rather than transition metals due to the complete filling of the d orbitals. Therefore, Pd_{13} exhibited a distorted icosahedron [21], while in a subsequent study the authors reported that two different density functionals can lead to two global minimum structures that are very close in energy and have the same spin states. The PBE functional has favoured the icosahedrons, whereas a structure that is similar to the one proposed by Wang and Johnson [22] has been preferred by the B3LYP functional.

Other theoretical studies using DFT-PBE calculations to study the electronic structure of Pd_{13} resulted in a bilayer structure which can be considered as a relaxed bulk fragment [23]. The icosahedral cluster was found to be slightly above the ground state, while stabilization by the p- or d-like cluster orbitals caused the near degeneracy of the bilayer or icosahedral clusters, respectively. The low-lying spin states were found to be important in controlling the electronic property of the cluster. Reveles and co-workers [24] used the linear combination of atomic orbitals-molecular orbital approach at the PBE/DZVP level of theory to learn the structural changes of bilayer C_S ground state and the octahedron of Pd_{13} upon charging and oxidation or reduction. It was observed that the bare Pd_{13} has C_S geometry, whereas $Pd_{13}O_2$ has an icosahedral Pd_{13} core (**Figure 4**), indicating an interesting structural change during an oxidation/reduction reaction. The location of 1P, 1D, and 2P cluster orbitals and the amount of hybridization between the atomic p orbitals and the cluster 1D orbitals determine the order of stability of the isomers.

DFT theory calculations within the spin-polarized generalized gradient approximation (GGA) were performed by Kumar and Kawazoe [25] to study the evolution of the atomic and electronic structure of Pd clusters having 2–23, 55, and 147 atoms. They observed that the binding

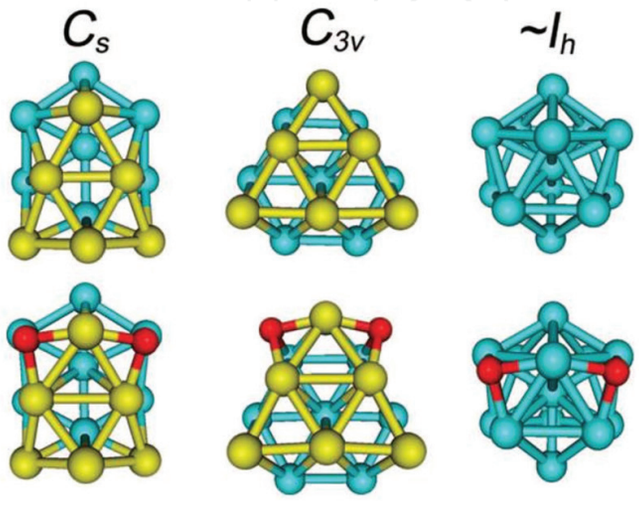

Figure 4. Topology of optimized Pd_{13} isomers (reproduced with permission from Ref. [24]).

energy increases monotonically toward the bulk value with the increasing cluster size. The 10-, 13-, 15-, 18-, 21-, and 22-atom clusters magic numbers were shown by the second-order energy differences. All of these arrangements show that numerous isomeric structures that are very close in energy were found for small Pd_n clusters $n \leq 15$, which prefer high spin states with small HOMO − LUMO gaps. Pd clusters having more than 100 atoms in the fcc arrangement showed higher cohesive energies than icosahedra and decahedra, suggesting a strong preference for the bulk packing.

4.2.2. Pt clusters

Platinum clusters have also been of keen interest due to their applications in catalysis. In most of the earliest investigations, semi-empirical methods were used and very small clusters such as dimers or trimers were studied due to limited computational resources. The self-consistent-field-Xα scattered wave (SCF-Xα-SW) approach to molecular orbital (MO) theory was used to study the electronic structure of Pt_{13} cluster with the cuboctahedral geometry [26]. The overlap of d-band by the s, p band and the sharp peak in the density of states around the Fermi level of Pt_{13} exhibited the main features of the Pt-bulk band structure. They also reported that the ionization potential of the Pt_{13} cluster is about 2 eV greater than the average bulk work function.

The PW91 level of theory along with a plane wave basis set has been used to study Pt clusters up to 55 atoms, and these systems have been compared for their stabilities and HOMO-LUMO gaps. Xiao and Wang [27] found that while the binding energy increases, the relative stability of the Pt clusters is not affected by the consideration of spin-orbit coupling. It was also discovered that out of several different isomers of 10-atom Pt clusters, the tetrahedral Pt_{10} is the most stable, while Pt_{55} is most stable in the icosahedral geometry.

However, a combined molecular dynamics simulations and DFT calculations study carried out to investigate the amorphization mechanism of icosahedral Pt nanoclusters was done by Apra et al. [28] using the Becke functional to describe exchange and Perdew-Wang functional for correlation with a Gaussian-type orbital (GTO) basis set. The authors proposed an amorphization mechanism of icosahedral (Ih) clusters, where the rosette-like structural excitations at the five-fold vertices take place. In the icosahedral 55-atom cluster, a vertex atom is inserted between the five neighbours on the surface, to form a six-fold ring centred on the original position of the vertex. The bond directionality effects due to d-d interactions increase the favourability of the rosette-like structure for Pt clusters.

4.2.3. Gold clusters

The study of gold has been of interest to researchers for many decades due to its wide variety of applications in catalysis, sensing and bio-tagging. The properties of gold nanoparticles and clusters are known to vary widely as the size of the system decreases so that the structures and properties of gold clusters are examined as a function of size.

The structures of pure gold clusters, especially the two-dimensional to three-dimensional structural transition have been the subject of many studies. The small clusters with fewer than 20 atoms were thoroughly investigated by several research groups [29, 30]. Some of the earliest work on large systems focused on symmetrical structures. Haberlen et al. [29]

examined octahedral and icosahedral Au_{55} using the Vosko, Wilks and Nusair (VWN) functional and found that the Kohn-Sham orbitals and their energy orderings agreed well with a jellium model once energy level splittings due to symmetry reduction were considered. Furthermore, it was found that relativistic calculations lowered the energy levels arising from s orbitals toward the d-band. Lately, examination of Oh-symmetric Au_{38}, Au_{44}, and Au_{55}, as well as Ih symmetric Au_{55} and Au_{147} showed that the VWN functional correlation predicts average gold–gold distances whose extrapolated values are in better agreement with experiment than BP86 [30]. However, the cohesive energies per atom were found to be better for BP86, while the energy differences between the two Au_{55} structures were found to be small, although the icosahedral structure was preferred by a factor less than 0.1 eV. Tetrahedral Au_{20} was also computed to have a HOMO-LUMO gap of 1.818 eV, which was in very good agreement with experimental estimates. Au_{40}, using a PBE-based basin-hopping search had that the lowest energy isomer with C_1 symmetry and a HOMO-LUMO gap of 0.69 eV [31, 32].

4.2.4. Silver clusters

Silver nanoparticles and clusters have many uses, some of which include optical sensing and surface enhanced Raman scattering (SERS). As a result, their structures, optical properties, and adsorbate binding have been studied by many researchers. Jennison et al. [33] examined Ag_{55}, Ag_{135}, and Ag_{140} with icosahedral and/or cuboctahedral structures using the Perdew-Zunger LDA parametrization. It was discovered that the icosahedral structures were energetically preferred. The central atoms in icosahedral structures were computed to have compressions in atomic distances of up to 6% as compared to bulk, but small surface compressions of ~1%, whereas the cuboctahedral structures were found to have core compressions of 1% and surface compressions of 2–3%.

The investigation of Ag_{55}^- using combined theory-experiment showed that the photoelectron spectrum of Ag_{55}^- was well-reproduced by an icosahedral structure, which was also found to be the lowest energy isomer for this cluster size [34]. But the structures of Ag_{55}^- and Ag_{55}^+ were later established using both DFT (BP86 with a SVP basis set) and trapped ion electron diffraction (TIED). Their reduced molecular scattering functions were found to be in excellent agreement with those predicted for icosahedral structures. The lowest energy isomer for Ag_{55}^- was predicted to be a slightly Jahn-Teller distorted singlet icosahedral structure; although a triplet state with D_{5h} symmetry was found to be almost isoenergetic [35].

A combination of TIED with DFT calculations was also employed using the PBE functional to examine Ag_n^+ (n = 36–46, 55). It was found that although clusters with fewer than 55 atoms exhibited local 5-fold symmetry in the absence of an icosahedral structure. In Ag_{38}^+, their ground-state structure had truncated octahedral symmetry, while their isomer that best fits the experimental data had 5-fold symmetry. The combined DFT and TIED study was expanded to investigate the structures of Ag_{19}^+, Ag_{38}^+, Ag_{55}^+, Ag_{59}^+, Ag_{75}^+, and Ag_{79}^+. The result was a truncated decahedral structure estimated to be 0.26 eV lower in energy than the truncated octahedral structure at the TPSS/TZVP level of theory [36].

The optical absorption spectrum of silver chains up to 18 atoms long was computed using real-time TDLDA calculations. It was found that the longitudinal excitation of the silver chains

http://dx.doi.org/10.5772/intechopen.72761

was not strongly affected by the presence of d electrons in the system, whereas the transverse plasmon modes were suppressed and mixed by the d electrons [37]. But studies conducted by means of statistical average of orbital potentials (SAOP) and XC functional of Van Leeuwen and Baerends (LB94) calculations showed that excitation of atomic wires in Ag_{20} and Ag_{40} demonstrated longitudinal peak arising primarily from a HOMO → LUMO transition, whereas the transverse excitation originates from a mixture of occupied-unoccupied orbital transitions [38].

5. The effects of the nanometer length scale

Once again, we recall the principle of quantum size effect as it directly influences the energy band structure which can lead indirectly to a number of changes in the associated atomic or crystal structure. These effects are generally termed quantum confinement, and they give rise to different observable changes in material properties.

The free electron model describes the energies of the electronic states as a function of $1/L^2$, where L is defined as the dimension of the system in a definite direction. The distance between successive energy levels is directly proportional to $1/L^2$. This property suitably describes a solid as a giant molecule. Therefore, the rate of increase in the number of atoms in the molecule results in decrease in molecular orbitals spacing. Therefore, if the number of atoms in a system, that is, the length scale, is considerably different from that in a bulk material, the energies and the energy spacing of the individual electronic states will be very different. Although the Fermi level (the upper most occupied level according to molecular orbital theory) would not be subject to change because the free electron density N/V would remain constant although there may be resultant modification in structure which will change this quantity. Invariably, decrease in the size of the system, causes the allowed energy bands to be considerably narrower than in an infinite solid. As a result, the delocalized electronic properties of a solid are remotely affected and the electrons in a reduced-dimensional system tend to behave more like the 'particle in a box' which is the phenomenon of 'quantum confinement'. The electronic states in such circumstances are more like those found in localized molecular bonds rather than those in a macroscopic solid [39].

Consequently, the total energy and thermodynamic stability of the reduced length scale system change relative to that of a normal bulk crystal, as a result of alterations to the bulk electronic structure provided that entropy consideration is negligible. Usually, this behaviour has important implications in the sense that it may change the most energetically stable form of a particular material, for example small nanoparticles and nano dimensional systems may adopt different crystal structures from that of the bulk material. Instances have shown that some metals which normally adopt a hexagonal close-packed atomic arrangement have been reported to adopt a face-centred cubic structure in confined systems such as metallic multilayers [40, 41]. If a different crystallographic structure is adopted below certain critical length scale, which is as a result of corresponding change in electronic density of states, it often results in a reduced total energy for the system.

The decrease in length scale may as well result in change in chemical reactivity, physical properties such as electrical, thermal, optical and magnetic characteristics, which depend on the structure and occupation of the outermost electronic energy levels. For instance, in a metallic system

there is a transition between metallic and insulation properties as the system size decreases, giving rise to the formation of a forbidden energy band gap. Other properties such as mechanical strength and transport properties which depend on change in the electronic structure and exhibition of a quantized behaviour respectively may also change in the length scale system [42].

5.1. Changes in the system structure

To understand the changes observed in systems of reduced dimension, let us consider the proportion of atoms which are in contact with either a free surface, for example an isolated nanoparticle, or an internal interface, such as a grain boundary in nanocrystallites. Therefore, the surface to volume ratio (S/V) and the specific surface area ($m^2\ g^{-1}$) of a typical system are indirectly proportional to particle size and they increase progressively for particles below 100 nm in diameter. The surface area per unit mass of material for isolated spherical particles of radius r and density ρ, is equal to

$$\frac{SA}{mass} = 4\pi r^2 \Big/ \left(\frac{4}{3\pi r^3 \rho}\right) = 3/r\rho \tag{2}$$

Therefore, the specific surface area (SSA) for 2 nm diameter spherical particles of typical densities can be approximately 500 $m^2\ g^{-1}$, but for particles forming crystals, the value will be reduced by half. The large surface area will definitely change the total energy of the system, leading to formation of metastable structures in nanosized systems that are different from the bulk structure and may induce a simple contraction or expansion of the normal crystalline lattice which could in turn change other material properties. For example, volume specific surface areas of 5 and 10 nm diameter spherical gold nanoparticles measured by the BET method were 342 and 316 m^2/cm^3 respectively [43], underscoring the quantum size effect.

For an atom that is near the surface, the number of nearest neighbouring atoms will be reduced thereby affecting bonding. Consequently, the surface tension or surface energy and electronic structure of the system will be affected. In a 2.5 nm particle only about 35–55% of the atoms are surface bound in contrast with a fewer percent for a 100 nm particle. This phenomenon applies mainly to nanocrystallites, most of their atoms either appear at or close to the grain boundaries and as a result, they exhibit structural properties different from the bulk [44].

5.2. Occurrence of vacancies in nanocrystals

This is another specific property that may control many physical properties such as conductivity and reactivity in materials. Vacancies are point defects in the crystalline structure of a solid, which exist in thermal equilibrium. In microcrystalline solids at temperatures above 0 K, vacancies invariably exist in thermal equilibrium. In the simple case of metals with one type of vacancies in a crystal having N atom sites is given by the Arrhenius equation

$$n_v = Nexp(^{-Q}/_{RT}) \tag{3}$$

where R is the gas molar constant, T is the absolute temperature and Q_f is the energy needed to form one mole of vacancies. Thus Q_f is given as

$$Q_f = N_A q_f \tag{4}$$

http://dx.doi.org/10.5772/intechopen.72761

where N_A is the Avogadro number and q_f is the activation energy for the formation of one vacancy. q_f is an estimation of the energy required to remove an atom from the interior of a crystal to its surface. Since a surface atom is considered to be bonded to half the number of atoms compared to an interior atom, therefore, q_f is approximately half the bonding energy per atom. q_f is expected to have a near linear function with the melting temperature T_m since T_m of a metal is a function of the bond energy, so alternatively, Q_f may be calculated from the surface energy per unit area if one atom occupies an area of b^2, then the number of atoms per unit area is equal to $1/b^2$ and the surface energy, σ is given as

$$\sigma = {}^{q}/_{b^2} \tag{5}$$

Surface energy is also a function of T_m and varies within the range 1.1 Jm^{-2} (for aluminium) to 2.8 Jm^{-2} (for tungsten). Assuming a mean value σ = 2.2 Jm^{-2} and b = 2.5 × 10^{-10} m, then

$$Q_f = N_A \sigma b^2 = 83\ x\ 10^3\ J\ mol^{-1} \tag{6}$$

This agrees with the acceptable value of 90 $KJmol^{-1}$. However, the contribution of internal pressure, P to the surface energy term σ may be employed to modify the value of Q_f for nanoparticles in the following expression: $P = 4\sigma/d$, where d is the diameter of the nanoparticle. The effect of P introduces another energy term, q_n, for the formation of a vacancy and is given as Pb^3. Again taking σ as 2.2 Jm^{-2}, the additional energy per mole $Q_n = N_A q_n$ which is equal to 8.3 × 10^3 $Jmol^{-1}$ for a 10 nm diameter nanoparticle. This term is only approximately 10% of Q_f and rapidly decreases for large particle sizes. Thus, the effect of surface energy and internal pressure on the concentration of vacancy will be minimal (**Table 1**). In addition, the internal pressure, P causes an elastic compressive volume strain which results in linear strain ε, given by

$$\varepsilon = P/3E = 4\sigma/3dE \tag{7}$$

Thus, E is the Young's modulus. This equation shows that linear strain is inversely proportional to particle size hence; there will be a decrease in lattice parameter or interatomic spacing for nanoscale dimensional particles.

Finally, substituting a value of Q = 90 × 10^3 $Jmol^{-1}$ into the Arrhenius expression for the vacancy gives the ratio n_v/N of 2.4 × 10^{-16} at 300 K, 6.5 × 10^{-7} at 600 K, 4.8 × 10^{-4} at 1000 K, depicting an exponential increase in vacancy concentration with temperature. In the case of a spherical

Metal	Surface energy, σ (eV) [45]	Specific surface area per atom, b^2 (m^2/cm^3)[a] [46]	T_m (°C)
Cu	1.29 ± 0.02	138.06	480
Ag	1.16 ± 0.02	124.15	480
Pt	1.62	312.62	480
Au	0.97 ± 0.01	104.89	480

[a]Calculated based on $\varepsilon = P/3E = 4\sigma/3dE$, assumption of d = 10 nm.

Table 1. Values of vacancy formation energy determined for copper, silver, platinum and gold (reproduced with permission from refs. [45, 46] As indicated).

nanoparticle of about 50 nm in diameter, if each atom occupies a volume of b^3, assuming $b = 0.25$ nm, there will be a total of 4.2×10^6 atoms in the particle. This implies that the number of vacancies, n_v very much less than 1 (except at very high temperature). Hence, nanocrystals are predictably vacancy free; their small size prevents any vacancy. This phenomenon has far reaching consequence for all thermo mechanical properties and chemical processes involving precipitation because they are based on the presence and migration of vacancies in the crystal lattice [47]. For instance gold nanowires having a diameter as small as 40 nm have a plastic deformation mechanism which is dominated by the motion of dislocations, a behaviour commonly observed in macro crystalline materials. As a result, the deformation mechanism of nanocrystalline gold films depends on its grain size [48].

5.3. Dislocation in nanocrystals

The mechanical properties of materials can be explained in terms of planar defects caused by dislocations in the crystalline structure of a solid. Dislocations plays less dominant role in the description of the properties of nanocrystals compared to microcrystals, due to the dominance of crystal surfaces and interfaces. The free energy of dislocation can be defined in terms of the following: (i) the core energy that is within a radius of about three lattice planes from the dislocation core; (ii) the elastic strain energy outside the core and extending to the boundaries of the crystal; and (iii) the free energy as a result of entropy contributions. It follows that, in microcrystals, the first and second terms which are the most dominant terms increase the free energy. Therefore, dislocations do not exist in thermal equilibrium making it different from vacancies. The core energy approximately 1 eV per lattice plane which, for an inter-planar spacing b of 0.25 nm, is equivalent to 6.5×10^{-10} Jm^{-1} is expected to be independent of grain size. The elastic strain energy per unit length for an edge dislocation is given by

$$E = \frac{G b^2}{4\pi(1-\nu)} x\, ln\left(\frac{r_1}{r_0}\right) \tag{8}$$

In this expression, G is the bulk modulus, r_0 is the core radius, r_1 is the crystal radius and ν is Poison's ratio, ν is usually around 1/3 for a crystalline sample. For a screw dislocation $(1-\nu)$ term is usually omitted, resulting in an energy approximately 2/3 that of an edge dislocation. If $G = 40 \times 10^9$ Pa, then the constant term $Gb^2/4\pi(1-\nu) = 3 \times 10^{-10}$ Jm^{-1}. The grain size dependence is the $ln(r_1/r_0)$ term, which for grain size $(2r_1)$ values of 10, 50, 1000 and 10,000 nm increases as 3, 4.6, 7.6 and 9.9 respectively. This suggests that, the elastic strain energy of dislocations in nanoparticles is almost one-third of that in microcrystals. For a 10 nm grain size, the core energy and elastic strain energy are not significantly different. In comparison, the core energy for a microcrystal is about one-tenth of the elastic strain energy.

The decrease in the elastic strain energy of dislocation in nanocrystals will invariably affect the forces of dislocations due to externally applied stresses; the interactive forces between dislocations will be reduced by a factor of about 10. Therefore, the rates of recovery and annealing out of dislocations to free surfaces are expected to be reduced. If there is a dislocation near the surface of a semi-infinite solid, the stress towards the surface will be defined as the interaction of the stress field of an image dislocation at an equal distance on the opposite side. Since nanocrystals do not approximate to semi-infinite solids, such image stresses will result in dislocations that are relatively immobile.

Further evaluation of the contributions of entropy to the free energy can be considered under the following conditions: (i) configurational entropy (that is, arrangement of the dislocation in different ways); (ii) entropy factor for a perfectly elastic dislocation by assumption; and (iii) the associated effect of dislocation on thermal vibrations of crystal. Interestingly, out of these three factors only (ii) and (iii) are not affected by crystal size and their values have been given as $2k_BT$ and $3k_BT$, respectively, per atomic plane. These values correspond to about 3×10^{-11} Jm^{-1}, considerably less than the core and elastic strain energy terms at a temperature of 300 K.

The configurational entropy contribution to the energy term is given as

$$E = \frac{b\,k_B\,T}{L}\,ln\left(\frac{L^2}{b^2}\right) \tag{9}$$

per atomic plane, where L is the length of the dislocation. At 300 K this gives values of 3.0×10^{-12}, 5.7×10^{-14} and 7.6×10^{-15} Jm^{-1} for $L = 10$, 1000 and 10,000 nm, respectively. In conclusion, unlike microcrystals, dislocations do not exist in nanocrystals as thermodynamically stable lattice defects [7, 49].

5.4. Effect of nanoscale dimensions on the properties of nanomaterials

Many properties of nanomaterials can be modified based on the length scale property (size). More often, extrinsic properties for example resistance, which depends on the actual size of the particle, may be affected. Whereas, other properties such as yield strength, τ solely depends on the microstructure of a material as expressed by the Hall–Petch equation for the material which is a function of average grain size (d)

$$\tau = k\,(d)^{-\frac{1}{2}} + \tau_0 \tag{10}$$

where k and τ_0 are constants. Resistivity which is an intrinsic material property is presumed to be independent of particle size, although this is usually not predictable for many intrinsic properties of matter at nanoscale compared to bulk phase due to the emergence of quantum size confinement resulting in the presence of wave-like transport processes, changes in electronic structure and the predominance of interfacial effects [50].

5.4.1. Effect on structural properties

The increase in surface area and surface free energy, with decreasing particle size leads to changes in interatomic spacing. This effect can be explained by the compressive strain induced by the internal pressure arising from the small radius of curvature in the nanoparticle. Furthermore, another effect previously mentioned is the apparent stability of metastable structures in small nanoparticles and clusters, such that all traces of the usual bulk atomic arrangement become lost. Metallic nanoparticles such as silver (**Figure 5a**, **b**, **d**), platinium (**Figure 5h**, **i**), palladium (**Figure 5e**, **f**), Co (**Figure 5g**), Ni (**Figure 5c**), ruthenium, gold (**Figure 6**) and some noble metals are known to adopt polyhedral shapes such as face centred cubic structure, cube-octahedra, multiply twinned icosahedra and multiply twinned decahedra.

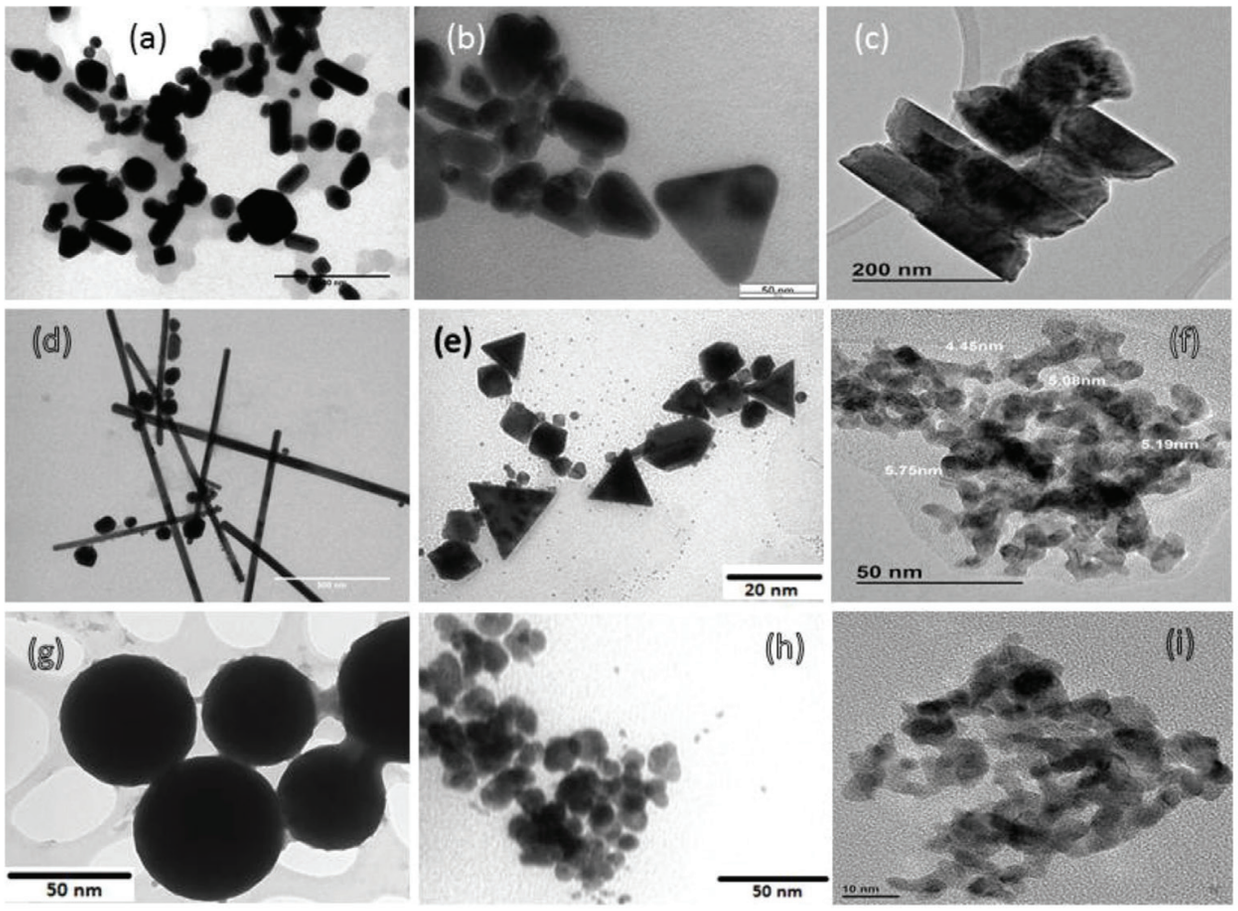

Figure 5. Transmission electron microscope (TEM) images of metal NCs: (a) face centered cubic and cube-octahedra Ag NCs; (b) multiple twinned Ag NCs; (c) disc-like Ni NCs; (d) Ag nanorods; (e) face centered hexoctahedral Pd NCs; (f) a dendritic Pd NC; (g) Co nanosphere; (h) hexoctahedral Pt NCs (i) Pt nanorods [51, 52].

Some of the nanoparticles are referred to as multiplied twinned crystalline particles (MTPs). Their shapes are considered based on the surface energies of various diffraction planes from x-ray diffraction (XRD) pattern, the growth rates of the crystals and the energy required to form defects such as twin boundaries. Moreover, evidence has shown that such particles are not true crystals but are referred to as quasiperiodic crystals or crystalloids. Some of these quasi nanostructures, icosahedral and decahedral quasicrystals (**Figure 5**) usually become seed for further growth of the nanocluster; until more regular crystalline packing arrangements are formed.

There is enormous difference between crystalline and amorphous solids in sense that the former possess long-range periodic order, their patterns and symmetries correspond to those of the 230 space groups. But quasiperiodic crystals do not exhibit such property; they possess fivefold-symmetry, which is not allowed in the 230 space groups. Some metals exhibit the cubic close-packed and hexagonal close-packed structures in which, each atom is coordinated by 12 neighbouring atoms. Although, other configurations exist in which each coordinating atom is situated at the vertices of an icosahedron while in contact with the central atom. Relaxing this rigid atomic model by allowing the central atom to reduce in diameter by ten percent (10%), the coordinating atoms shift position and the shape and symmetry of a regular icosahedron forms with point group symmetry 235, indicating the presence of 30 twofold, 20 threefold and 12 fivefold axes of

http://dx.doi.org/10.5772/intechopen.72761

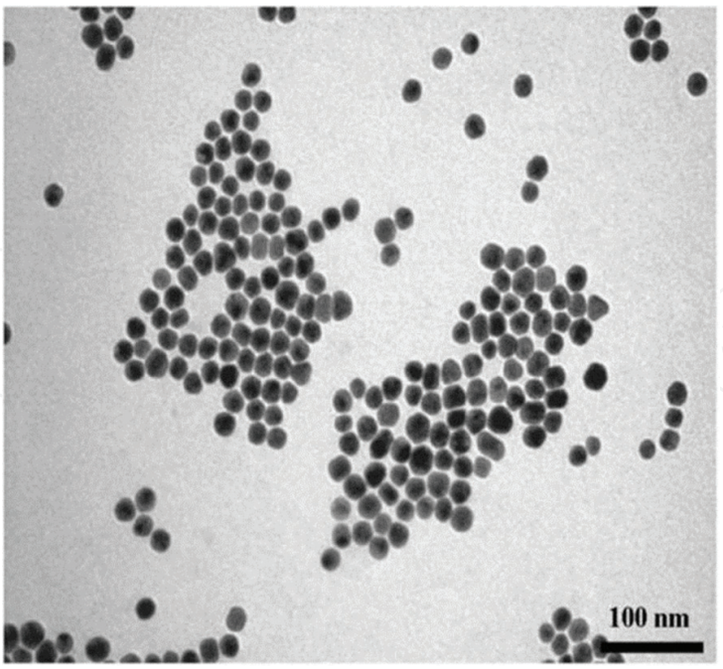

Figure 6. Face centered cubic structure au NCs (reproduced with permission from Ref. [53]).

symmetry. This kind of geometry of a quasiperiodic crystal nucleus may grow to form icosahedra or pentagonal dodecahedra. In these two solids having identical symmetry; the apices of one are replaced by the faces of the other, but the understanding of their size-related instability characteristics and mechanism still remains unclear. More often, electron diffraction pattern is employed to distinguish between multiple twinned crystals and quasiperiodic crystals [54].

5.4.2. Effect on thermal properties

The perceived large increase in surface area and the change in interatomic spacing as a function of nanoparticle size as mentioned earlier, have a marked effect on material properties. For metallic nanoparticles, the smaller the size the higher the melting point. But there is a correlation between the size functionality of metal nanoparticles, their plasmon resonance behaviour arising from electron–electron/electron phonon couplings and conductivity which is related to thermal dissipation or release of heat energy to the environment.

Specifically, the relationship between the size, temperature and the surface plasmon energy of silver nanoparticles (size range 11–30 nm) embedded in a silica host matrix has been studied for the temperature interval 293–650 K. This study confirmed the dependence surface plasmon energy on the size and temperature of silver nanoparticles [55]. An increase in temperature and size of nanoparticle, shifts the surface plasmon resonance band to the red side of the spectrum. A decrease in the size of nanoparticles invariably results in increase in the rate of scattering of surface conduction electrons and leading to a nonlinear red shift of the surface plasmon resonance. This temperature dependence of SPR energy and its red shift is linear for larger nanoparticles but is nonlinear for smaller ones. Therefore, the volume thermal expansion of nanoparticles leads to a red shift of the surface plasmon resonance at higher temperature. It also reveals that the thermal volume expansion coefficient depends on size and temperature.

5.4.3. Effect on chemical properties

There is a relationship between change in structure as a function of particle size and electronic properties. Ionization energy of small atomic clusters is higher than the corresponding bulk material. In addition, ionization energy remarkably varies with cluster size, which is also related to chemical reactivity.

It has been established that nanoscale structures have very high surface area to volume ratio and possess varying crystallographic structures which has implication for chemical reactivity. Therefore, catalysts consisting of finely divided nanoscale system can increase the rate, selectivity and efficiency of chemical reactions while simultaneously significantly reducing waste and pollution in the sense that only a few quantity of the material as catalyst is required to be deposited on a support inside a reactor and it can be used repeatedly. Once the cycle of usage or lifetime is spent, it can be recharged and reused again. Similarly, the ease of transport to and from internal reaction sites can be enhanced by employing nanoscale catalytic support with nanoporous structure which selects the reactants and product of chemical reactions based on size. In addition, the solubility property of nanoparticles often differs from their bulk counterparts, for example, while some new drugs in micron-sized particle form may be insoluble in water, but when nanostructured, they easily dissolve because of improved permeability occasioned by increased surface to volume ratio. Also, the reduced particle size renders the possibility of intravenous administration of poorly soluble drugs without any blockade of the blood capillaries. The suspensions can also be lyophilized into a solid matrix [56–59].

5.4.4. Effect on mechanical properties

It well known that toughness as a mechanical property is inversely proportional to ease of formation or defects within a material. Therefore, as particle size decreases, the ability to sustain defects becomes increasingly more difficult which will alter mechanical properties. So it expected that new nanostructures that are different from their bulk materials in terms of morphology and structure will definitely show different mechanical properties. As the structural scale reduces to the nanometer range, for example in nanolayered composites, based on the Hall-Petch relationship, yield strength apparent increases. Furthermore, the high surface to volume ratio of nanostructured materials may also promote interface-driven processes such as plasticity, ductility and strain to failure. Several nano metals and ceramics are known to be superplastic, because they are capable of undergoing extensive deformation process without necking or fracture as a result of grain boundary diffusion and sliding, which is very significant in nanosized materials. Therefore, these effects offer an advantage in the sense that the strength-ductility limit of novel nanomaterials is extended over that of the conventional materials [60].

5.4.5. Effect on magnetic properties

The large surface area to volume ratio effect also results in a substantial proportion of atoms having a different magnetic coupling with neighbouring atoms leading to a variation in magnetic properties. Some important applications of magnetic nanoparticles include bioprocessing, colour imaging, ferrofluids, refrigeration and high storage density magnetic memory media. **Figure 4** shows average magnetic moments per atom of metal clusters such as Fe (**Figure 7a**),

http://dx.doi.org/10.5772/intechopen.72761

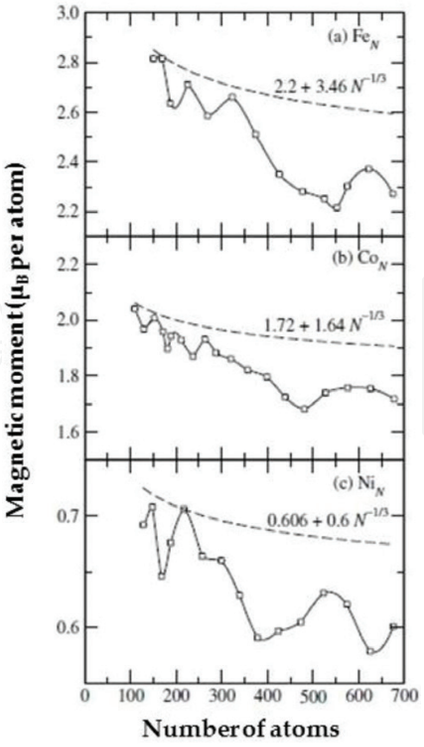

Figure 7. Average magnetic moment per atom for (a) Fe clusters at 120 K, (b) co clusters at 78 K, and (c) Ni clusters at 78 K, as a function of the number of atoms (reproduced with permission from Ref. [61]).

Co (**Figure 7b**) and Ni (**Figure 7c**) at different temperature. Bulk ferromagnetic materials often form characteristic multiple magnetic domains, while small magnetic nanoparticles usually exhibit only one domain and possess superparamagnetism [62].

Other related effect in this regard is giant magnetoresistance (GMR) which is observed in nanoscale multilayers consisting of a strong ferromagnet, such as Fe and Co and a weaker magnetic or nonmagnetic buffer (Cr and Cu). It is used in data storage and sensing. Another unique feature of GMR is the ability to produce different spin alignments with or without a magnetic field which result in antiferromagnetic coupling leading to maximum scattering from the interlayer interface and hence a high resistance parallel to the layers. The reverse occurs for co-aligned spins which results in decreased resistance of the device [63].

5.4.6. Effect on optical properties

The resultant effect of reduced dimensionality in nanocluster on electronic structure is profound in semiconductors as a result of the interaction between the highest occupied molecular orbital (HOMO) also called the valence band, and the lowest unoccupied molecular orbital (LUMO), known as the conduction band. Optical absorption and emission depend on transition between these states leading to changes their optical properties, such as colour which is as a function of particle size. A very good example of variation of colour with particle size is colloidal silver nanoparticles. It has a light yellow colour which progressively becomes more yellowish with increase in particle size. Since the seventeenth century silver colloids have been

used as a pigment for stained glass. Most metallic nanoparticles show similar size-dependent behaviour in terms of frequency and intensity of light emission and modified non-linear optical properties. Reduced dimensionality also has effect on photoemission, photoconductivity, photocatalysis and electro-luminescence [64, 65].

5.4.7. Effect on electronic properties

The effect of reduced dimensionality on the electronic properties of the system is related mainly to the increasing influence of the wave-like property of the electrons and the paucity of scattering centres. The discrete nature of the energy states become apparent in systems that are confined in all three dimensions due to quantum mechanical effect based on de Broglie wavelength theory. In addition, owing to their intrinsic wave-like nature, electrons can form tunnel by quantum mechanical effect between two closely adjacent nanostructures. If a voltage is applied between these two nanostructures which align the discrete energy levels in the DOS, resonant tunnelling occurs, leading to abrupt increase in tunnelling current (this phenomenon is different from simple dipolar coupling which results from each electron spin generating a magnetic field that is oriented parallel to the nuclear spin vector).

As a result, below a critical length scale, conducting materials may become insulators, as the energy bands cease to overlap. Whereas in bulk materials, electronic transport is mainly determined by scattering caused by phonons, impurities or rough interfaces. At nanoscale dimension electron motion can be diffusive and become purely ballistic if the electron free path can travel through the system without randomization of the phase of their wavefunction. This principle operates in superconductors. Conduction in highly confined structures like quantum dots is very sensitive to the presence of charge carriers. These Coulomb blockade effects result in conduction processes involving single electron which only requires a small amount of energy to operate a transistor, switch or memory device. These devices can be utilized to produce state of the art components for electronic, optoelectronic and information processing applications, such as resonant tunnelling transistors and single-electron transistors [16, 42, 66]. We provide an illustration of this phenomenal critical length scale considering the work of Yao et al. [67] in which X-ray absorption fine structure, XAFS, was employed to look at the bonding between gold atoms. The ideal theoretical calculated gold bond length was within the range of 2.55–2.70 Å for gold nanoparticles which is much shorter than the bulk bond length of 2.87 Å [68].

6. Application of metallic nanoparticles

Metal nanoparticles have host of applications ranging from electronic, optical, magnetic imaging, biomedical therapy, catalysis and many more. The ultimate goal of their application is to explore the intrinsic physical and chemical properties of the colloidal nanoparticle whether in isolated or combined form to fabricate devices with specific functionality. In view of this, different strategies such as solvent evaporation, electrostatic attraction, hydrogen bonding, DNA-driven assembly, and cross-linking induced by bio-specific interaction like antigen–antibody and so on have been developed to form NP assemblies and utilize them in the fabrication of nanostructured devices. The utilization of quantum dots as functional materials

due to their extremely small size and extra high fluorescence quantum yield, [69] is however hampered as a result of their toxicity potential in biomedical applications. Meanwhile, metallic NPs have enjoyed increased application in this regard [70].

6.1. Therapeutic in-vivo applications

The use of metallic nanoparticles in biomedical can be classified based on their mode of application inside (in-vivo) or outside (in-vitro) the body. The in-vivo application can be further characterized as therapeutic (hyperthermia and drug-targeting) and diagnostic (nuclear magnetic resonance, NMR imaging). The main divisions of the in- vitro application involve magneto relaxometry and diagnostic separation or selection.

6.1.1. Hyperthermia therapeutic method

This is a therapeutic procedure administered to raise the temperature of part of the body infected by a malignant tumour or cancerous growths. Hyperthermia therapy is usually applied together with other cancer treatments, and the technique is known as multimodal oncological strategies. Clinical examination has shown that at temperatures above 41–42°C, target cells can be mortified. Recent development in clinical hyperthermia trials now seeks to optimize thermal homogeneity at controlled temperatures between 42 and 43°C in the target volume. Among other methods, finely divided iron cobalt magnetic nanoparticles have used to deliver the temperature increase required for hyperthermia. In theory, magnetic hyperthermia, which is the controlled heating of a cell by a magnetic material under the influence of an external alternating magnetic field, occurs as a result of the loss processes associated with reorientation of the magnetization of magnetic materials with low electrical conductivity. This procedure functions by restricting the heating to the tumour area, which serves as a useful advantage in medical therapy. In recent times, the use of subdomain magnetic particles (nanosized) is preferred over multi domain (micronsized) particles, because the former absorb much more AC magnetic fields. Therefore, morphological properties such as particle size and shape are strong determinants of the heating potential of magnetic nanoparticles; that is why synthetic routes must be defined to produce uniform particles with particle size within the length scale regime [71, 72].

6.1.2. Drug delivery

The application of magnetic nanoparticles for the delivery of drugs or antibodies to organs or tissues infected by diseases is an interesting field of research with challenging opportunities. The process of drug transport to target site using magnetic delivery systems depends on the competition between forces exerted by blood compartment on the particles and magnetic forces generated from the applied magnet field. For magnetic particles to be retained at the target site, the magnetic forces must exceed the linear blood flow rates in arteries (10 cms^{-1}) or capillaries (0.05 cms^{-1}). Therefore, the pioneering concept proposed by Freeman and coworkers [73] which suggests that fine magnetic carrier particles could be transported through the vascular system and be concentrated at a particular point in the body with the aid of a magnetic field (**Figure 8a**) has be validated. The main advantage of this procedure is that the transport of nanoparticles through capillary systems, organs and tissues is favoured, so that vessel embolism could be prevented [75].

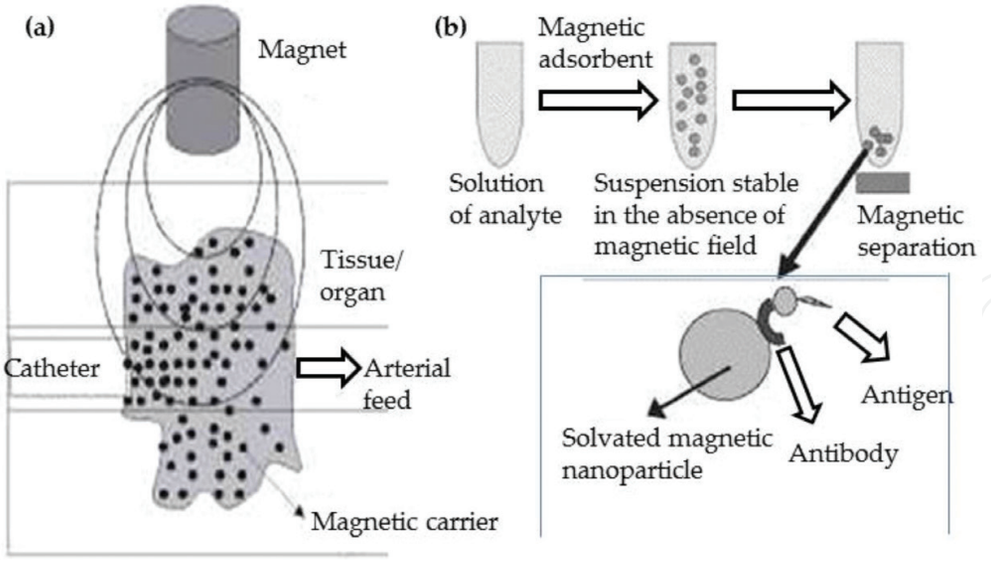

Figure 8. (a) Schematic diagram of magnetically driven transport of drug to a specific target and (b) representation of a magnetically assisted separation of substances. Magnetic nanosphere to which an antibody has been anchored is dispersed into a liquid medium containing antigen (reproduced with permission from Ref. [74]).

6.2. Diagnostic in-vitro applications

6.2.1. Separation and selection

Solid phase extraction (SPE) is a viable alternative to the conventional sample separation or concentration methods, for example, liquid–liquid extraction. At present, considerable attention is being paid to SPE as a means of isolating and pre-concentrating desired components from a sample matrix. The separation and pre-concentration of the substance from large volumes of solution is highly time consuming when using standard SPE column, but with the advent of magnetic adsorbents in magnetic solid-phase extraction (MSPE) this task can be made relatively easier. Using this procedure, the magnetic adsorbent is added to a suspension or solution containing the target material, which is adsorbed onto the magnetic adsorbent and then desorbed or recovered from the suspension by using an appropriate magnetic separator (**Figure 8b**). The use of magnetic nanoparticles instead of micronsized magnetic particles in this procedure is of advantage because suspensions that are resistant to sedimentation can be prepared in the absence of an applied magnetic field [76].

6.2.2. Magnetorelaxometry

Magnetorelaxometry is a procedure that measures the magnetic viscosity or the relaxation of the net magnetic moment of a system of magnetic nanoparticles after withdrawal of a magnetic field. This method was recently introduced for the evaluation of immunoassays. It uses two different relaxation mechanisms: (i) Néel relaxation occurs if the internal magnetization vector of a nanoparticle relaxes in the direction of the easy axis inside the core: and (ii) Brownian relaxation occurs if the particles accomplish rotational diffusion in a carrier liquid. Both Néel and Brownian relaxations can be identified by their individual relaxation times. Other distinguishing properties include, Brownian relaxation only takes place in liquids, while Neel

relaxation does not depend on dispersion medium. Since magneto-relaxometry is a function of particle core size, hydrodynamic size and particle anisotropy, the technique can effectively distinguish between free and bound conjugates by their unique magnetic behaviour. As a result, it can be used as an analytical tool for the evaluation of immunoassays [77, 78].

6.2.3. Future applications of magnetic nanoparticles

Tremendous effort has been made to contribute to research in the field of magnetic therapeutic medicine. Magnetically directed microspheres containing radionuclides are currently used for internal radiotherapy. There is a need to improve dose localization when administering drugs and metabolites which have been labelled with radioactive isotopes in a quantity sufficient to deactivate tumour cells. Therefore, the use of capped magnetic nanoparticles could have tremendous impact in improving the efficiency cancer treatments. Sufficient advance in magnetic nanoparticles research could evolve into their use in human body repair called prosthetics or artificial replacement [79].

7. Conclusions

In this review, the periodic properties of both crystalline and amorphous solids have been discussed as well as their unique physical and chemical properties at nanoscale level with their corresponding applications. Metallic nanoparticles and nano-layers have very high surface area to volume ratio and potentially different crystallographic structures which result in their unique physical and chemical reactivity both as solids and as colloidal dispersions.

Author details

Joseph Adeyemi Adekoya[1,3]*, Kehinde Olurotimi Ogunniran[1],
Tolutope Oluwasegun Siyanbola[1], Enock Olugbenga Dare[2] and Neerish Revaprasadu[3]

*Address all correspondence to: yemidunni20022001@gmail.com

1 Department of Chemistry, Covenant University, Ota, Ogun, Nigeria

2 Department of Chemistry, Federal University of Agriculture, Abeokuta, Nigeria

3 Department of Chemistry, University of Zululand, KwaDlangezwa, South Africa

References

[1] Brian LC, Vladimir LK, Charles JO. Recent advances in the liquid-phase syntheses of inorganic nanoparticles. Chemical Reviews. 2004;**104**:3893-3946

[2] Jonathan WS, David RT, Karl JW. Core Concepts of Supramolecular Chemistry and Nanochemistry. England: John Wiley and Sons Limited; 2007

[3] John PL. Quantum Chemistry. Student ed. London: Academic Press Incorporated; 1978

[4] Gary LM, Donald AT. Inorganic Chemistry. 3rd ed. London: Pearson Education International; 1998. pp. 337-520

[5] Roco MC, Williams RS, Alivisatos P. Nanotechnology Research Directions. 2nd ed. Dordecht: Kluwer Press; 2000. pp. 71-111

[6] Robert GM. Physical Chemistry. 3rd ed. Burlington: Elsevier Academic Press; 2008. pp. 108-240

[7] Robert WK, Lan WH, Mark G, editors. Nanoscale Science and Technology. 1st ed. England: John Wiley and Sons Limited; 2005. pp. 15-220

[8] Gohlich H, Lange T, Bergmann T, Martin TP. Electronic shell structure in large metallic clusters. Physical Review Letters. 1990;**65**(6):748-751

[9] Rubio-Bollinger G, Balm SR, Agrait N, Jacebsen KW, Vieira S. Mechanical properties and formation mechanism of a wire of single gold atoms. Physics Review Letters. 2001; **87**(02):6101

[10] Plain J, Sonnefraud Y, Viste P, Lérondel G, Huant S, Royer P. Self assembly drives quantum dot photoluminescence. Journal of Fluorescence. 2009;**19**(2):311-316

[11] Levy B. Photochemistry of nanostructured materials for energy applications. Journal of Electroceramics. 1997;**1**(3):239-272

[12] Törmä P, Barnes WL. Strong coupling between surface plasmon polaritons and emitters: A review. Reports on Progress in Physics. 2015;**78**:013901 (34 pp)

[13] Horst-Gunter R. Basics of Nanotechnology. 3rd revised ed. London: Wiley-VCH; 2008. pp. 10-13

[14] Xiukai L, Shuxin O, Naoki K, Jinhua Y. Novel Ag_2ZnGeO_4 photo catalyst for dye degradation under visible light irradiation. Applied Catalysis A: General. 2008;**334**:51-58

[15] Hammond C. The Basics of Crystallography and Diffraction. London: Oxford University Press; 1997. pp. 119-254

[16] Kolasinkin KW. Surface Science: Foundation of Catalysis and Nanoscience. Chichester: Wiley-VCH; 2002. pp. 43-65

[17] van Leeuwen R, Baerends EJ. Exchange-correlation potential with correct asymptotic behavior. Physical Review A. 1994;**49**:2421-2431

[18] Reddy BV, Khanna SN, Dunlap BI. Giant magnetic moments in 4d clusters. Physical Review Letters. 1993;**70**:3323-3326

[19] Estiu GL, Zener MCJ. Interplay between geometric and electronic structure and the magnetism of small Pd clusters. The Journal of Physical Chemistry. 1994;**98**(18):4793-4799

[20] Watari N, Ohnishi S. Atomic and electronic structures of Pd_{13} and Pt_{13} clusters. Physical Review B. 1998;**58**:1665-1677

[21] Sun Y, Zhang M, Fournier R. Periodic trends in the geometric structures of 13-atom metal clusters. Physical Review B. 2008;**77**:075435-075438

[22] Wang LL, Johnson DD. Density functional study of structural trends for late-transition-metal 13-atom clusters. Physical Review B. 2007;**75**:235405-235410

[23] Köster AM, Calaminici P, Orgaz E, Roy DR, Reveles JU, Khanna SN. On the ground state of Pd_{13}. Journal of the American Chemical Society. 2011;**133**:12192-12196

[24] Reveles JU, Köster AM, Calaminici P, Khanna SN. Structural changes of Pd_{13} upon charging and oxidation/reduction. The Journal of Chemical Physics. 2012;**136**:114505-114506

[25] Kumar V, Kawazoe Y. Evolution of atomic and electronic structure of Pt clusters: Planar, layered, pyramidal, cage, cubic, and octahedral growth. Physical Review B. 2008;**77**:205418-205410

[26] Messmer RP, Knudson SK, Johnson KH, Diamond JB, Yang CY. Molecular-orbital studies of transition- and noble-metal clusters by the self-consistent-field-Xα scattered-wave method. Physical Review B. 1976;**13**(4):1396-1415

[27] Xiao L, Wang L. Structures of platinum clusters: Planar or spherical? Journal of Physical Chemistry A. 2004;**108**:8605-8614

[28] Apra E, Baletto F, Ferrando R, Fortunelli A. Amorphization mechanism of icosahedral metal nanoclusters. Physical Review Letters. 2004;**93**(6):065502-065504

[29] Haberlen OD, Chung SC, Rösch N, Rösch N. Relativistic density-functional studies of naked and ligated gold clusters. International Journal of Quantum Chemistry. 1994;**52** (28 S):595-610

[30] Haberlen OD, Chung S-C, Stener M, Rösch N. From clusters to bulk: A relativistic density functional investigation on a series of gold clusters Au_n n = 6,…,147. The Journal of Chemical Physics. 1997;**106**(12):5189-5201

[31] Hakkinen H. Atomic and electronic structure of gold clusters: Understanding flakes, cages and superatoms from simple concepts. Chemical Society Reviews. 2008;**37**:1847-1859

[32] Garzón IL, Beltrán MR, Posada-Amarillas A, Ordejón P, Artacho E, Sánchez-Portal D, Soler JM. Lowest energy structures of gold nanoclusters. Physical Review Letters. 1998;**81**(8):1600-1603

[33] Jennison DR, Schultz PA, Sears MP. Ab initio calculations of Ru, Pd, and Ag cluster structure with 55, 135, and 140 atoms. The Journal of Chemical Physics. 1997;**106**(5):1856-1862

[34] Hakkinen H, Moseler M, Kostko O, Morgner N, Hoffmann MA, von Issendorff B. Symmetry and electronic structure of Noble-metal nanoparticles and the role of relativity. Physical Review Letters. 2004;**93**(9):093401-093404

[35] Schooss D, Blom MN, Parks JH, Issendorff BV, Haberland H, Kappes MM. The structures of Ag55+ and Ag55−: Trapped ion electron diffraction and density functional theory. Nano Letters. 2005;**5**(10):1972-1977

[36] Blom MN, Schooss D, Stairs J, Kappes MM. Experimental structure determination of silver cluster ions ($Ag_{(n)}$+, 19 < or = n < or = 79). The Journal of Chemical Physics. 2006;**124**(24):244308-244310

[37] Yan J, Gao S. Plasmon resonances in linear atomic chains: Free-electron behavior and anisotropic screening of *d* electrons. Physical Review B. 2008;**78**:235413-235410

[38] Guidez EB, Aikens CM. Theoretical analysis of the optical excitation spectra of silver and gold nanowires. Nanoscale. 2012;**4**:4190-4198

[39] Wenxin N, Guobao Y. Review: Crystallographic control of Noble metal nanocrystals. Nano Today. 2011;**6**:265-285

[40] Zheng J, Nicovich PR, Dickson RM. Highly fluorescent Noble metal quantum dots. Annual Review of Physical Chemistry. 2007;**58**:409-431

[41] Melnikov G, Emelyanov S, Ignatenko N, Ignatenko G. The quantization of the radii of coordination spheres cubic crystals and cluster systems. IOP Conference Series: Materials Science and Engineering. 2016;**110**:012065

[42] Rao CNR, Muller A, Cheetham AK. The Chemistry of Nanomaterials; Properties and Applications. Weinheim: Wiley-VCH Verlag GmbH and Co.; 2004. pp. 12-49

[43] EAF VD, PRH DT, MAD F, Mast J. Determination of the volume-specific surface area by using transmission electron tomography for characterization and definition of nanomaterials. Journal of Nanobiotechnology. 2011;**9**(17):8

[44] Feynman R. There's plenty of room at the bottom. Engineering Science. 1992;**23**:22

[45] Triftshiiuser W, McGervey JD. Monovacancy formation energy in copper, silver, and gold by positron annihilation. Applied Physics. 1975;**6**:177-180

[46] Gao P, Wu Q, Li X, Ma H, Zhang H, Volinsky AA, Qiao L, Su Y. Size-dependent concentrations of thermal vacancies in solid films. Physical Chemistry Chemical Physics. 2016;**18**:22661-22667

[47] Goldstein AN. Handbook of Nanophase Materials. Vol. 3. New York: Marcel Dekker; 1997. pp. 105-301

[48] Korkin A, Rosei F, Lockwood DJ, editors. Nanoelectronics and Photonics: From Atoms to Materials, Devices, and Architectures. New York: Springer Science & Business Media; 2008

[49] Suryanarayana C, Singh J, Froes FH, editors. Processing and Properties of Nanocrystalline Materials. Warrendale: TMS; 1996

[50] Poole CP, Owens FJ. Introduction to Nanotechnology. New Jersey: Wiley-VCH; 2003. pp. 1-23

[51] Adekoya JA, Dare EO, Ogunniran KO, Siyanbola TO, Akinsiku AA, Ehi-Eromosele CO, et al. Facile route to synthesize organically capped size controlled silver nanoparticles. International Journal of Scientific & Engineering Research. 2014;**5**(3):1220-1226

[52] Adekoya JA, Dare EO, Ogunniran KO, Siyanbola TO, Ajani OO, Ehi-Eromosele CO, et al. Tandem synthesis of some low and high indexed monometallic nanoparticles in polyols, poly(vinylpyrrolidone), trisodium citrate and dodecanethiol matrices. Digest Journal of Nanomaterials and Biostructures. 2015;**10**(4):1311-1327

[53] Sosibo NM, Keter FK, Skepu A, Tshikhudo RT, Revaprasadu N. Facile attachment of TAT peptide on gold monolayer protected clusters: Synthesis and characterization. Nanomaterials. 2015;**5**(3):1211-1222

[54] Jurgen O, Rainer G, Rolf EJ, Marc A, Frank G, Kirill K, et al. Palladium-gallium intermetallic compounds for the selective hydrogenation of acetylene. Part 1: Preparation and structural investigation under reaction conditions. Journal of Catalysis. 2008;**258**:210-218

[55] Yeshchenko OA, Dmitruk IM, Alexeenko AA, Kotko AV, Verdal J, Pinchuk AO. Size and temperature dependence of the surface plasmon resonance in silver nanoparticles. Ukrainian Journal of Physics. 2012;**57**(2):266-277

[56] Tan N, Zhou ZY, Sun SG, Ding Y, Wang ZL. Synthesis of tetrahedral platinum nanocrystals with high index facets and high electro-oxidation activity. Science. 2007;**316**:732-735

[57] Tan N, Zhou ZY, Sun GS. Electrochemical preparation of Pd nanorods with high-index facets. Chemical Communication. 2009;**45**:1502-1504

[58] Tan N, Zhou ZY, Yu NF, Wang LY, Sun GS. Direct electrodeposition of tetrahedral Pd nanocrystals with high-index facets and high catalytic activity for ethanol electro-oxidation. Journal of America Chemical Society. 2010;**132**:7580-7581

[59] Patel VR, Agrawal YK. Nanosuspension: An approach to enhance solubility of drugs. Journal of Advanced Pharmaceutical Technology and Research. 2011;**2**(2):81-87

[60] Edelstein AS, Cammarata RC. Nanomaterials: Synthesis, Properties and Applications. 2nd ed. London: CRC Press, Taylor and Francis Group; 1998

[61] Xie Y, Blackman JA. On the oscillation of the magnetic moment of free transition metal clusters. Journal of Physics: Condensed Matter. 2003;**15**:L615-L622

[62] Carcia PF, Shah SI, Zeper WB. Effect of energetic bombardment on the magnetic coercivity of sputtered Pt/co thin-film multilayers. Applied Physics Letters. 1990;**56**(23):2345-2347

[63] Marickam M. Electronic magneto-thermal properties of ferromagnetic clusters. Journal of Physics and Chemistry of Solids. 2005;**66**:977-983

[64] Janos HF, editor. Nanoparticles and Nanostructured Films-Preparation, Characterization and Applications. New York: Wiley-VCH; 1998

[65] Moffit M, McMahon L, Pessel V, Eisenberg A. Size control of nanoparticles in semiconductor-polymer composites, 2: Control via sizes of spherical ionic microdomains in styrene based diblock ionomers. Chemistry of Materials. 1995;**7**:1185-1192

[66] Wells AF. Structural Inorganic Chemistry. 4th ed. London: Oxford University Press; 1975. pp. 74-120

[67] Yao T, Sun Z, Li Y, Pan Z, Wei H, Xie Y, Nomura M, Niwa Y, Yan W, Wu Z, Jiang Y, Liu Q, Wei S. Insights into initial kinetic nucleation of gold nanocrystals. Journal of the American Chemical Society. 2010;**132**(22):7696-7701

[68] Thanh NTK, Maclean N, Mahiddine S. Mechanisms of nucleation and growth of nanoparticles in solution. Chemical Reviews. 2014;**114**:7610-7630

[69] Biju V, Itoh T, Anas A, Sujith A, Ishikawa M. Semiconductor quantum dots and metal nanoparticles: Syntheses, optical properties, and biological applications. Analytical and Bioanalytical Chemistry. 2008;**391**:2469-2495

[70] Nikolai GK, Lev AD. Optical properties and biomedical applications of plasmonic nanoparticles. Journal of Quantitative Spectroscopy and Radiative Transfer. 2010;**111**:1-35

[71] Charles SW, Popplewell J. Properties and applications of magnetic liquids. In: Buschow KHJ, editor. Hand Book of Magnetic Materials. Vol. 2. UK: Wiley Publisher; 1986. p. 153

[72] Rosensweig RE. Heating magnetic fluid with alternating magnetic field. Journal of Magnetism and Magnetizable Materials. 2002;**252**:370-374

[73] Freeman MW, Arrot A, Watson HHL. Structure in vitreous silicate fibers as shown by small–angle scattering of x-rays. Journal of Applied Physics. 1960;**31**:404

[74] Tartaj P, del Puerto Morales M, Veintemillas-Verdaguer S, Gonzalez-Carreno T, Serna CJ. The preparation of magnetic nanoparticles for applications in biomedicine. Journal of Physics D: Applied Physics. 2003;**36**:R182-R197

[75] Goodwin S, Peterson C, Hoh C, Bittner C. Targeting and retention of magnetic targeted carriers (MTCs) enhancing intra-arterial chemotherapy. Journal of Magnetism and Magnetizable Material. 1999;**194**:132-139

[76] Safarikova M, Safarik I. Magnetic solid phase extraction. Journal of Magnetism and Magnetizable Materials. 1999;**194**:108-112

[77] Rheinlander T, Kotitz R, Weitschies W, Semmler W. Magnetic fractionation of magnetic fluids. Journal of Magnetism and Magnetizable Materials. 2000;**219**:219-228

[78] Coombs RRH, Robinson DW, editors. Nanotechnology in Medicine and Bioscience. Vol. 3. New York: Gordon and Breach; 1996

[79] Dailey JP, Phillips JP, Li C, Riffle JS. Synthesis of silicone magnetic fluid for use in eye surgery. Journal of Magnetism and Magnetizable Material. 1999;**194**:140-280